AGU100 ADVANCING EARTH AND SPACE SCIENCE

Water Resources Research

RESEARCH ARTICLE

10.1029/2018WR022950

Key Points:

- A downscaling technique links rainfall statistics at a point with areal averages from remotely sensed data sets
- Extreme value statistics at a point are estimated using the Metastatistical Extreme Value distribution
- The method can be used for the validation of rainfall statistics derived from satellite-borne measurements

Correspondence to:
E. Zorzetto,
enrico.zorzetto@duke.edu

Citation:
Zorzetto, E., & Marani, M. (2019). Downscaling of rainfall extremes from satellite observations. *Water Resources Research*, *55*, 156–174. https://doi.org/10.1029/2018WR022950

Received 14 MAR 2018
Accepted 19 NOV 2018
Accepted article online 26 NOV 2018
Published online 8 JAN 2019

Downscaling of Rainfall Extremes From Satellite Observations

Enrico Zorzetto[1] and Marco Marani[1,2,3]

[1]Division of Earth and Ocean Sciences, Duke University, Durham, NC, USA, [2]Department of Civil and Environmental Engineering, Duke University, Durham, NC, USA, [3]Dipartimento di Ingegneria Civile, Edile ed Ambientale, Universita' degli studi di Padova, Padova, Italy

Abstract The estimation of the frequency of intense rainfall events is a crucial step for quantifying their impact on human societies and on the environment. This process is hindered by large gaps in ground observational networks at the global scale, such that extensive areas remain ungauged. The increasing availability of satellite-based rainfall estimates, while providing data with unprecedented resolution and global coverage, also introduces new challenges: the scale disparity between gridded and rain-gauge precipitation products on the one hand, and the short length of the available satellite records on the other. Here we propose a statistical framework for the estimation of rainfall extremes that is specifically designed to simultaneously address these two key issues, providing a new way of estimating extreme rainfall magnitudes from space. A downscaling procedure is here introduced to recover the spatial correlation and the probability density function of daily rainfall at the point (gauge) scale from coarse-scale satellite estimates. The results are then combined with a recent statistical model of extremes (the Metastatistical Extreme Value distribution), which optimizes the use of the information obtained from relatively short satellite observational time series. The methodology is tested using data from the Tropical Rainfall Measuring Mission Multisatellite Precipitation Analysis over the Little Washita River, Oklahoma. We find that our approach satisfactorily reproduces downscaled daily rainfall probability density functions and can significantly improve the Tropical Rainfall Measuring Mission Multisatellite Precipitation Analysis-based estimation of quantiles with return times larger than the length of the available data set (19 years here), which are especially important for several water-related applications.

1. Introduction

Even though systematic rainfall observations date back more than two centuries (Camuffo et al., 2013; Marani & Zanetti, 2015; Ntegeka & Willems, 2008), and rain-gauge networks are quite developed internationally (Menne et al., 2012), the global density of rainfall observations still exhibits large gaps over continents (Kidd et al., 2016), with oceans remaining largely ungauged. In recent decades, advances in rainfall remote sensing technologies have contributed to attenuate this chronic lack of spatial information and have made available vast rainfall data sets, with unprecedented resolution in space and time. Rainfall satellite estimates from different sensors (chiefly radar, microwave imagery, and infrared sensors) are now routinely combined to produce global grids of quantitative precipitation estimates (QPEs). Satellite-derived QPEs, and in particular, observations from the Tropical Rainfall Measuring Mission (TRMM; Huffman et al., 2007) and the Global Precipitation Measurement mission (Huffman et al., 2014), greatly improve our knowledge of global precipitation dynamics, with implications for a wide variety of water-related disciplines, from water resources engineering, to risk evaluation and management, to ecology and eco-hydrology.

However, the quantification of the accuracy associated with satellite QPEs encounters a basic difficulty in their comparison with reference observations at the ground. In most cases, sufficiently accurate rainfall observations that are long enough for validating QPE extreme values are only available at the rain-gauge scale, thus preventing a direct comparison. How the statistical properties of a rainfall field change as it is averaged spatially has been investigated both from the point of view of random processes (Bell, 1987; Cowpertwait et al., 2002; Cox & Isham, 1988; Marani, 2005; Vanmarcke, 1983) and using the formalism of random cascades (Gupta & Waymire, 1993; Nogueira & Barros, 2015; Over & Gupta, 1996; Schertzer & Lovejoy, 1987). However, the central problem for QPE validation remains developing relations between the properties of rainfall averaged over coarse spatial scales (as in the case of remote sensing QPEs, with common resolutions varying between 10^1 and 10^2 km^2), to those measured at a point in space.

Given the important implications associated with an accurate quantification of rainfall from space, calibrating, testing, and quantifying uncertainty in satellite QPEs using rain-gauge data are important open problems (Hossain & Huffman, 2008; Libertino et al., 2016; Müller & Thompson, 2013; Pan et al., 2010; Villarini & Krajewski, 2007), and in particular the comparison of ground-based radar and satellite sensor statistics has been object of extensive research. Kirstetter et al. (2012) introduced a framework to evaluate the performance of space-borne precipitation sensors based on ground radar mosaics. They proposed a weighted average of ground radar observations, which accounts for the power gain function of the space-borne sensor, assumed to be Gaussian. Gebremichael and Krajewski (2004) investigated to what extent radar-derived rainfall products can capture small-scale rainfall variability. They employed a point to area conversion of the correlation function and found that radar-estimated correlations tend to be lower than those observed by rain gauges at spatial distances shorter than 5 km.

Müller and Thompson (2013) proposed a bias correction procedure for TMPA 3b42 QPEs based on a stochastic representation of the rainfall field. Rainfall statistics observed at measuring stations are interpolated and used to estimate properties of the rainfall field at the TMPA pixel scale and correct TMPA QPEs accordingly. While the method can be used for extrapolations to ungauged pixels, its calibration requires observations from a sufficiently large number of measurement stations within the same TMPA pixel to fit the stochastic model to the rainfall field. A downscaling technique that only makes use of TMPA-measured rainfall statistics (mean, variance, and number of wet days) was proposed by Del Jesus et al. (2015) based on a simple stochastic model of point rainfall (Cox & Isham, 1988). While the proposed technique does not require knowledge of ground information for its calibration, the assumptions made on the point rainfall process (chiefly, the exponential distribution of rainfall duration and intensity) hinder its application to the study of rainfall extremes.

The estimation of extreme rainfall return levels is particularly affected by the uncertainty and measurement errors that characterize space-borne rainfall retrievals and is further hindered by the short observational coverage provided by satellite sensors (currently less than 20 years for TRMM and Global Precipitation Measurement retrievals). Under these premises, the quantification of the frequency of occurrence of rainfall extremes is inherently difficult, as large quantiles are, by definition, poorly sampled in short observational time series. What is more, traditional extreme value analyses, based on the use of just annual maxima (AM), or of relatively few values over a high threshold (Coles et al., 2001), discard most of the information contained in already short QPE time series and are thus extremely sensitive to the observational uncertainty of a small number of observations. As a result, standard extreme value analyses applied to QPE data are inevitably affected by large and difficult to quantify uncertainties, that severely limit its use for quantitative predictions (Zhou et al., 2015).

The examination of the literature points to significant gaps in (1) relating the statistics of rainfall observed at coarse spatial scales with those observed at a point and (2) the use of remote sensing observations to derive extreme rainfall properties. The main objective of the present manuscript is to bridge these gaps by introducing a novel statistical downscaling methodology with specific focus on extreme rainfall statistics. To this end, we build a framework that (1) relates daily rainfall statistics from area-integrated remote sensing QPEs to those from point measurements at the ground and (2) infers extreme rainfall statistics via the Metastatistical Extreme Value distribution (MEVD; Marani & Ignaccolo, 2015; Marra et al., 2018; Zorzetto et al., 2016). This approach simultaneously addresses the issues related to the short sample sizes and to the coarse spatial resolution of satellite QPEs. MEVD links the probability distribution of extreme events to the entire underlying distribution of "ordinary" daily events, here defined as all the daily rainfall accumulations greater than a fixed and low threshold. The MEVD approach has been shown to significantly reduce estimation uncertainty, with respect to traditional extreme value analysis methods, particularly for values of the average recurrence interval (*Return Time*, T_r) larger than the length of the time series used for calibration (Zorzetto et al., 2016). Furthermore, MEVD estimates are defined using the entire set of observations, rather than just a portion of the distributional tail, and thus produce estimates that are less sensitive to the observational uncertainty and to the presence of outliers in QPE data sets. Marra et al. (2018) recently tested the MEVD framework using synthetic rainfall time series perturbed with errors typical of satellite observations. They found that MEVD is more robust to these sources of error than traditional extreme value models, thus supporting this first application of the method to satellite QPEs.

This MEVD-based downscaling methodology is here presented and tested using TRMM TMPA Research Version 7 3b42 QPEs over the Little Washita watershed, Oklahoma, where the dense Micronet rain gauge network allows an accurate description of the spatial distribution of rainfall (Elliott et al., 1993; Villarini & Krajewski, 2007; Villarini et al., 2009).

2. Materials and Methods

The instantaneous rainfall rate at the ground can be regarded as a three-dimensional random field $i(x, y, t)$, described by a suitable set of coordinates (here t indicates time, and x and y are the rectangular coordinates of a point on Earth's surface). Both rain gauges and remote sensing observations provide an integral representation of $i(x, y, t)$ on a finite space-time domain centered at a point (x_c, y_c, t_c), which can in general be expressed as

$$h_L(x_c, y_c, t_c) = \frac{1}{L_x L_y} \int_{x_c-\frac{L_x}{2}}^{x_c+\frac{L_x}{2}} \int_{y_c-\frac{L_y}{2}}^{y_c+\frac{L_y}{2}} \int_{t_c-\frac{T}{2}}^{t_c+\frac{T}{2}} i(x, y, t)dxdydt \tag{1}$$

where the rainfall intensity $i(x, y, t)$ is averaged over a rectangular spatial domain, with sides L_x and L_y, and is integrated over a time interval T. For example, in the case of traditional rain gauges, the rainfall volume is recorded as an integral over finite time intervals (e.g., hourly or daily), while the measurement can be regarded as being performed at point in space, given the small integration area (order of 10^{-2} m^2). Conversely, the reflectivity fields retrieved by a radar may be regarded as average values over a spatial domain corresponding to the size of a radar beam (order of square kilometers). For example, retrievals by the precipitation radar on board the TRMM mission are best interpreted as weighted averages within each radar beam, with weights that depend on the characteristics of the sensor (Kirstetter et al., 2012). The time scale of a radar retrieval is very short, as it is the result of the quasi-instantaneous detection of hydrometeors within layers of the atmospheric column. Here we focus our attention on TMPA multisensor products, which can be regarded as pixel-average QPEs, and perform our analyses on precipitation retrievals aggregated at the fixed daily time scale ($T_d = 24$ hr)

$$h(x, y) = \int_{t_c-\frac{T_d}{2}}^{t_c+\frac{T_d}{2}} i(x, y, t)dt \tag{2}$$

so as to investigate the effects of spatial averaging alone on the statistical properties of satellite-sensed rainfall fields. To this end, in the next subsections (i) we introduce a framework for linking the daily rainfall distribution at a point and its counterpart averaged over an area of a given size, (ii) we present a methodology for inferring the correlation structure of the rainfall field from satellite QPEs, and (iii) we combine this information to estimate the MEVD at a point in space from satellite area-averaged observations.

2.1. Scale-Wise Variation of the Distribution of Daily Rainfall

The occurrence of daily rainfall at a point can be described by a stochastic process alternating between dry and wet states. The probability distribution of this compound process is characterized by a finite atom of probability in zero and its moments, in particular, its mean μ_{c_0} and variance $\sigma^2_{c_0}$, differ from the corresponding statistics of the wet process only (nonzero rainfall, with mean and variance μ_{r_0} and $\sigma^2_{r_0}$ respectively). Here the first subscript refers either to the *compound* process (c) or to the wet (rainfall being detected) component only (r), while the second subscript distinguishes the process at a point ($_0$) from the process averaged at the spatial scale of satellite retrievals (L). L is a characteristic linear scale of the satellite pixel measurement, defined as the square root of the pixel area ($L = \sqrt{L_x L_y}$). While we are interested in the distribution of "wet" events when studying extremes, it is necessary to also consider the compound process as rainfall observations averaged at large scales also include zero-rainfall areas.

For the compound process, the reduction of variance connected with the spatial averaging of the rainfall field can be expressed by a variance function of the form

$$\gamma_0(L) = \frac{\sigma^2_{c_L}}{\sigma^2_{c_0}} = \frac{4}{L_x^2 L_y^2} \int_0^{L_x} \int_0^{L_y} \left(L_x - x\right)\left(L_y - y\right) \rho(x, y)dxdy \tag{3}$$

where $\sigma^2_{c_L}$ is the variance of the (compound) rainfall field averaged in a space domain of area $A = L_x \cdot L_y$ corresponding to the QPE pixel size, $\sigma^2_{c_0}$ is its variance at a point and $\rho(x, y)$ is the spatial correlation function of the process, here assumed to be quadrant symmetric (Vanmarcke, 1983). While γ_0 in general depends on the shape of the area over which the average is carried out, here we apply the method to TMPA time series, and therefore, we assume that γ_0 only depends on the linear characteristic scale of the TMPA pixel, L.

10.1029/2018WR022950

The intermittent nature of rainfall fields implies that not only the variance of the process (and its higher-order moments) but also the yearly number of wet days N_L of the averaged process will in general differ from the yearly number of wet days N_0 observed at a point, as it is possible to have a pixel-averaged value of rainfall greater than zero when only part of the pixel is actually wet (Villarini et al., 2008). Here we characterize this effect by introducing an *intermittency function* β_0, defined as the ratio between the probability of the pixel of size L being wet, p_{r_L}, and the probability of any given point inside it being wet p_{r_0}, that is, $\beta_0(L) = p_{r_L}/p_{r_0}$.

We require that the average of the rainfall process must remain constant when averaging in space, so that $\mu_{c_L} = \mu_{c_0}$, as a consequence of the conservation of mass. However, the average of the wet process will not in general be conserved across scales, such that

$$\mu_{r_0} = \mu_{r_L}\beta_0 \tag{4}$$

Analogously, the variance of the intermittent rainfall process can be linked to the variance of the wet events by means of the following relation, that holds at any spatial scale (see Appendix A for its derivation)

$$\sigma_c^2 = \sigma_r^2 p_r + \mu_r^2\left(1 - p_r\right)p_r \tag{5}$$

whence using the definition of the variance function γ_0 from equation (3) we obtain

$$\sigma_{r_L}^2 p_{r_L} + \mu_{r_L}^2\left(1 - p_{r_L}\right)p_{r_L} = \gamma_0\left[\sigma_{r_0}^2 p_{r_0} + \mu_{r_0}^2\left(1 - p_{r_0}\right)p_{r_0}\right] \tag{6}$$

and thus, using equations (4) and (6), one can obtain the statistics of the point process in terms of area-averaged quantities

$$\sigma_{r_0}^2 = \frac{\beta_0}{\gamma_0}\left[\sigma_{r_L}^2 + \mu_{r_L}^2\left(1 - p_{r_L}\right)\right] - \mu_{r_0}^2\left(1 - p_{r_0}\right) \tag{7}$$

Several parametric distributions have been proposed to model the nonzero daily rainfall accumulations, ranging from exponential-type distributions to stable distributions (e.g., see Gnedenko & Kolmogorov, 1954; Menabde & Sivapalan, 2000). Here we employ a Weibull distribution to describe the wet component of the daily rainfall process across spatial scales. We note that (i) the Weibull distribution has been found to appropriately describe daily rainfall across many different climates globally, while sharing a formal analogy with the multiplicative nature of convective processes (Frisch & Sornette, 1997; Wilson & Toumi, 2005), and (ii) the Weibull distribution describes both light- and heavy-tailed random variates with characteristic scale through a parsimonious two-parameter model (Laherrere & Sornette, 1998). However, we note that the approach we propose here is quite general and can be tailored to processes characterized by different two-parameter distributions with only minor modifications.

The Weibull distribution is here parameterized with a scale parameter C and a shape parameter w, so that the cumulative probability distribution of the random variable H_L, representing daily rainfall accumulations at the spatial scale L, reads $P(H_L < h_L) = 1 - \exp\left[-\left(h_L/C_L\right)^{w_L}\right]$. The first two central moments of this distribution (i.e., its mean and variance) are respectively

$$\mu_{r_L} = \frac{C_L}{w_L}\Gamma\left(\frac{1}{w_L}\right) \tag{8}$$

and

$$\sigma_{r_L}^2 = \frac{C_L^2}{w_L^2}\left[2w_L\Gamma\left(\frac{2}{w_L}\right) - \Gamma\left(\frac{1}{w_L}\right)^2\right] \tag{9}$$

where Γ denotes the Gamma function. Equation (4) applied to the case of a Weibull variate yields a relation linking the shape and scale parameters of the process at two different scales

$$\left(\frac{C_0}{w_0}\right)^2 = \beta_0^2\left(\frac{C_L}{w_L}\right)^2\frac{\Gamma^2\left(\frac{1}{w_L}\right)}{\Gamma^2\left(\frac{1}{w_0}\right)} \tag{10}$$

A similar argument can be applied for the variance of the compound process, defined in equation (7), using the expression for the Weibull moments (equations (8) and (9)) and equation (10)

$$\gamma_0\beta_0 \frac{2w_0\Gamma\left(\frac{2}{w_0}\right)}{\Gamma^2\left(\frac{1}{w_0}\right)} = \frac{2w_L\Gamma\left(\frac{2}{w_L}\right)}{\Gamma^2\left(\frac{1}{w_L}\right)} + \left(\gamma_0 - 1\right) p_{r_L} \tag{11}$$

Equation (11) is nonlinear and can be solved numerically to determine the value of the shape parameter, w_0, at a point in space. Finally, equation (10) yields the value of the scale parameter C_0 at a point. This procedure can be used to infer the parameters of the probability distribution of nonzero rainfall values (the "wet process") at a point from the parameters describing the distribution of area-averaged values, provided the values of γ_0 and β_0 are known.

Here we define a *wet day* (i.e., a day in which an "ordinary" rainfall event occurs) as a 24-hr period characterized by rainfall amounts greater or equal to $q = 1$ mm. This threshold value is assumed constant across spatial scales and different data sources. Defining wet days using a fixed and low threshold is necessary when applying the method to data from both rain gauges and satellite sensors, which are inherently characterized by different detection thresholds. The 1-mm threshold value is coherent with the guidelines by the World Meteorological Organization (Klein Tank et al., 2009). The analysis proceeds by applying the Weibull distribution of ordinary daily rainfall accumulations to the excess above the threshold, $y = h - q$. We note that the distribution of y corresponds to the distribution of the rainfall accumulations h conditional to being above threshold: $P(Y \leq y) = P(H \leq y + q|H > q)$. Accordingly, the number of wet events and their statistics are computed for the population above this detection threshold.

We also note that the above argument can be extended to link the pdf of daily rainfall between two spatial scales L_1 and L_2, with, for example, $L_1 > L_2$. In this case, the ratios of the variance and wet fraction of the process averaged at these two spatial scales can be respectively expressed as $\gamma(L_1, L_2) = \gamma_0(L_1)/\gamma_0(L_2)$ and $\beta(L_1, L_2) = \beta_0(L_1)/\beta_0(L_2)$. Next, we explore how the value of the two ratios, γ_0 and β_0, can be estimated from satellite retrievals.

2.2. A Model for the Correlation Structure of Daily Rainfall

The equations relating the Weibull distributional parameters at a point in space to those valid for areal-averaged rainfall (equations (10) and (11)) require knowledge of the variance function γ_0 (equation (3)), which, in turn, depends on the correlation structure $\rho(x, y)$ of the rainfall field. Relating the correlation structure of the continuous stochastic field (whose realizations are the rain gauge point observations) to that of the same field averaged over finite areas (whose realizations are the satellite QPEs) requires additional attention to the issue of spatial scale. In fact, spatial averaging does not only affect the probability distribution of rainfall daily totals, but it also modifies the correlation between their values at two points in space when their distance is commensurate with the characteristic length scale L of the averaging area.

The covariance between the local averages h_L and h'_L of the precipitation field performed over two different pixel areas with the same characteristic size L can be expressed as (Vanmarcke, 1983)

$$Cov\left[h_L, h'_L\right] = \frac{\sigma^2_{c_0}}{4\left(L_x L_y\right)^2} \sum_{k=0}^{3} \sum_{l=0}^{3} (-1)^k (-1)^l \triangle \left(L_{x,k}, L_{y,l}\right) \tag{12}$$

where $\sigma^2_{c_0}$ is the variance of the process at a point, and the quantities $\triangle(L_{x,k}, L_{y,l})$ are the analogues of the variance function in equation (3) valid for the integral of the random field over a finite area of sizes $L_{x,k}$ and $L_{y,l}$

$$\triangle \left(L_{x,k}, L_{y,l}\right) = 4 \int_0^{L_{x,k}} \int_0^{L_{y,l}} \left(L_{x,k} - s_1\right) \left(L_{y,l} - s_2\right) \rho(s_1, s_2) ds_1 ds_2 \tag{13}$$

The set of distances $L_{x,k}$ and $L_{y,l}$ (with $k, l = 0, 1, 2, 3$) encodes all the necessary information on the relative position of the two pixels over which the averages of the rainfall field are computed. If Δx and Δy are the distances, along the x and y direction respectively, between the centers of two pixels, $L_{x,k}$ is defined as

- $L_{x,0} = \Delta x - L_x$ (distance between the end of the first pixel and the beginning of the second, along coordinate x)
- $L_{x,1} = \Delta x$ (distance between the beginning of the first pixel and the beginning of the second, along the coordinate dimension x)

- $L_{x,2} = \Delta x + L_x$ (distance between the beginning of the first pixel and the end of the second, along the coordinate dimension x)
- $L_{x,3} = \Delta x$ (distance between the end of the first pixel and the end of the second, along the coordinate dimension x)

Analogous definitions hold for $L_{y,l}$ along the y direction.

The expression of the covariance (equation (12)) can be used to obtain the correlation, ρ_{h_L,h'_L}, between the two pixel-averaged time series as a function of their relative position:

$$\rho_{h_L,h'_L} = \frac{Cov[h_L, h'_L]}{\sigma_{h_L}\sigma_{h'_L}} = \frac{\sum_{k=0}^{3}\sum_{l=0}^{3}(-1)^k(-1)^l \triangle(L_{x,k}, L_{y,l})}{4\triangle(L_x, L_y)} \tag{14}$$

where the covariance of local averages has been divided by the variances σ_{h_L} and $\sigma_{h'_L}$ of the process averaged over the two pixels respectively.

If a parametric analytical expression is available for the correlation $\rho(x, y)$ of the precipitation field at a point, then equation 14 can be used to determine its parameters by matching the right hand side with the inter-pixel correlation observed from a satellite-sensed rainfall field. Note that, under the hypothesis of an isotropic rainfall field, the two-point correlation $\rho(x, y)$ only depends on the distance between two points in space, so that it can be expressed as a function $\rho(d)$ with $d = \sqrt{x^2 + y^2}$.

Here we use a correlation structure characterized by an exponential kernel (EK) and a power-law tail (Marani, 2003).

$$\rho(d) = \begin{cases} e^{-\frac{\alpha d}{\epsilon}} & d < \epsilon \\ \left(\frac{\epsilon}{ed}\right)^{\alpha} & s \geq \epsilon \end{cases} \tag{15}$$

This expression is continuous with continuous derivative in $d = \epsilon$, and can describe both light- and heavy-tailed families of correlation decay. In the following, we apply this model to test the ability of equation (14) of reproducing the variation in the rainfall spatial correlation between the satellite pixel and the point scale.

The spatial correlation of the process averaged at the pixel scale is obtained by directly computing the value of the Pearson correlation coefficient between pairs of TMPA pixels located at different distances. While the Pearson correlation is known to be a possibly biased estimator when applied to a skewed and intermittent process such as rainfall (Habib et al., 2001), alternative estimates would require ad hoc hypotheses on the rainfall distribution and on the conditional probability of zero rainfall (Villarini et al., 2008). We therefore choose to use the classic Pearson correlation estimator, which entails the minimal number of additional assumptions.

If n_s TMPA grid cells are used in the estimation of the spatial correlation, $m = n_s(n_s - 1)/2$ estimates of the correlation (ρ_j, for $j = 1, 2, \ldots m$) are obtained, each corresponding to a distance d_j between the centers of the pair of pixels considered. The TMPA-observed spatial correlation is then assumed to match the correlation function of the area-averaged process, given by equation (14), which depends on the unknown parameters ϵ and α defining the point correlation function. A sum of square errors (SSE) is computed as

$$SSE(\epsilon, \alpha) = \sum_{j=1}^{m}\left[\rho_{h_L,h'_L}\left(d_j; \epsilon, \alpha\right) - \rho_j\right]^2 \tag{16}$$

The quantity $SSE(\epsilon, \alpha)$ in equation (16) is then minimized using the *L-BFGS-B* algorithm (Byrd et al., 1995) to obtain a best estimate of the parameters (ϵ, α). Once the correlation function at a point is known, it can be used in equation (3) to compute the variance reduction function, $\gamma_0(L)$, necessary to obtain the distribution of rainfall accumulations at a point.

When computing the variance and covariance of local averages (equations (3) and (14)) we assume a square pixel so that $L_x \simeq L_y \simeq L$. Therefore, $\gamma_0 = \gamma_0(L)$ is simply a function of the linear characteristic scale L of the pixel.

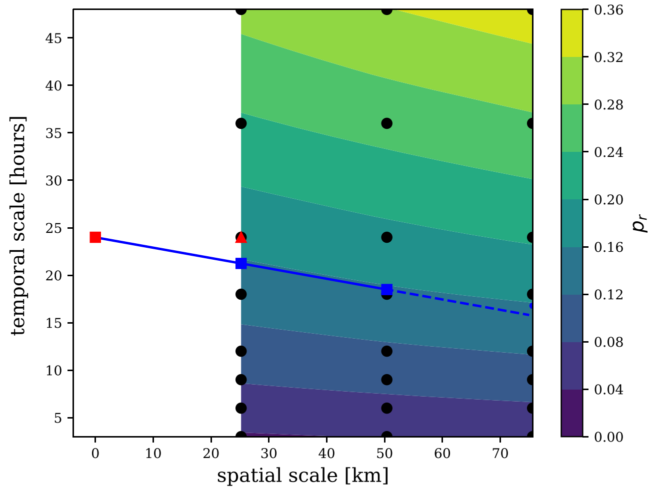

Figure 1. Extrapolation of the wet fraction at different integration scales. The black circles represent scales in space and time at which Tropical Rainfall Measuring Mission Multisatellite Precipitation Analysis (TMPA) 3b42 precipitation estimates are aggregated. The density plot shows interpolated p_r values within the range of scales covered by the TMPA product. Blue squares represent the points used to compute the local advection velocity (slope of the blue line), and the red square shows the target scale at which extrapolation of p_r is performed (rain gauge measurement). The red triangle shows the time-space scale of the TMPA pixel-average time series, used to compute the β_0 ratio.

2.3. Downscaling of the Yearly Number of Rainfall Events

The last piece of information necessary to reconstruct the pdf of daily rainfall at a point is the ratio β_0, which accounts for the variation in the yearly number of rainfall events when the rainfall field is averaged over the pixel area. Here we propose an application of *Taylor's Frozen Turbulence Hypothesis* (Taylor, 1938) to use TMPA information at finer temporal resolution (down to 3 hr) to infer the subpixel scale intermittency of the rainfall process at the daily scale. The Taylor hypothesis has been previously applied to study the space-time scaling of rainfall fields (e.g., Deidda, 2000) and was employed by Haerter et al. (2015) to compare precipitation products at different spatial scales. Here we apply a similar argument to estimate the spatial wet fraction of the compound rainfall field from its variability in time as inferred from TMPA 3b42 data only.

When applied to rainfall measurements, the Taylor hypothesis states that statistical properties of the rainfall field sampled at a spatial aggregation scale X and instantaneously in time are equivalent to the same properties sampled at a temporal scale $T = X/U$ and at a point in space, where U has the meaning of an average "advection" speed. Therefore, according to this hypothesis, properties of the field (such as the wet fraction p_r of the compound rainfall process), when advected past a rain gauge, do not change significantly over time. This assumption holds, for example, for turbulent flows characterized by small turbulent intensity (i.e., the root-mean-squared longitudinal velocity fluctuation must be small compared to the mean advection speed) (Stull, 1988).

If the Taylor hypothesis holds exactly, then the contour lines where $p_r(X, T)$ is constant are straight lines in (X, T) space. More generally, the advection velocity may vary with the aggregation scale of the process, consistent with the rainfall process being described by a multifractal field (Eggert et al., 2015). Following this assumption, we define an advection velocity U as the ratio between differences of integration scales in space and time respectively that would produce the same observed difference in the quantity p_r.

Here we estimate the wet fraction p_r using the TMPA 3b42 precipitation time series integrated at different temporal (T = 3, 6, 9, 12, 24, 36, and 48 hr) and spatial scales ($X = L, 2L, 3L$, corresponding to local averages over one TMPA pixel, 2×2 and 3×3 pixels respectively), as shown in Figure 1. The measured values of p_r are then interpolated in time (here using n_p = 1,000 values of the temporal scale T in the range from 3 to 48 hr), and the local slope of the p_r contour levels is used to estimate the local advection velocity U.

We select a target aggregation scale (X_G, T_G) (e.g., the aggregation scale in space and time of rain gauge measurements) and identify the unique values $\hat{X}_0$ and $\hat{U}$ such that the line $X = \hat{X}_0 + \hat{U} \cdot T$ passes through the target scale and has a slope equal to the local advection speed. The local advection speed is evaluated as the slope between two points with spatial aggregation scales $X = L$ and $X = 2L$ (corresponding to the local averages over 1 pixel and 2 × 2 pixels, respectively) and temporal scales determined by two conditions: (i) the two points share the same value of the observed wet fraction $p *_r$ and (ii) when extrapolating to the rain gauge scale, the resulting line passes through the target scale (X_G, T_G) (blue line in Figure 1). These two conditions together uniquely determine the two quantities $\hat{X}_0$ and $\hat{U}$ and thus can be used to compute the unknown property p_r^* at the rain gauge scale simply extrapolating TMPA observations. The intermittency function can then be evaluated as $\beta_0 = p_r(L, T_d)/p_r^*$, that is, as the ratio between the wet fraction at the 1-pixel, daily-scale $p_r(L, T_d)$, and the wet fraction p_r^* extrapolated at the rain gauge scale (X_G, T_G). This procedure assumes that the contour lines of the wet fraction in the (X, T) plane can be approximated to straight lines for spatial scales smaller than $2L$.

2.4. Extreme Value Model

We have seen how our hypotheses on the spatial structure of the rainfall fields yield a model for the marginal distribution of daily rainfall at a point. This information can now be used to estimate rainfall extremes. We base our analysis on the MEVD (Marani & Ignaccolo, 2015; Zorzetto et al., 2016), which expresses the cumulative distribution function of block-maxima, $\zeta(h)$, of independent variates ("ordinary values") distributed according to an underlying parent distribution with cumulative probability function $P(H \le h) = F(h; \vec{\theta})$, as

$$\zeta(h) = \sum_{N=0}^{\infty} \int_{\Omega_{\vec{\theta}}} g(N, \vec{\theta}) F(h; \vec{\theta})^N d\vec{\theta} \tag{17}$$

where $\vec{\theta}$ is the set of parameters describing the parent distribution $F(h, \vec{\theta})$, $\Omega_{\vec{\theta}}$ is their population, N is the number of events/block, and $g(N, \vec{\theta})$ is the joint probability density function of N and $\vec{\theta}$. In order to avoid ad-hoc assumptions about the expression for $g(N, \vec{\theta})$ (Zorzetto et al., 2016), we use a sample mean in place of the ensemble mean when evaluating (17) from a sample time series of s years. We further adopt, as customary in extreme precipitation analysis, 1-year blocks, and, for $F(h; \vec{\theta})$, a Weibull distribution, such that the $\vec{\theta} = (C, w)$ and the MEVD cumulative distribution function of yearly maxima becomes

$$\zeta(h) = \frac{1}{s} \sum_{j=1}^{s} \left[1 - e^{\left(-\frac{h}{C_j}\right)^{w_j}} \right]^{N_j} \tag{18}$$

where Weibull parameters and number of wet days (C_j, w_j, N_j) are allowed to vary across years. Zorzetto et al. (2016) extensively study the properties of MEVD and find, over a large data set of long daily rain-gauge time series, that it significantly reduces extreme-value estimation uncertainty with respect to traditional approaches hinged on the Generalized Extreme Value distribution when only relatively small samples (with respect to the return time of interest) are available for calibration. In the present context, the parameters of the Weibull distributions in equation (17) are estimated for each year on record ($j = 1, 2, \dots, s$) from the TMPA data set and then downscaled to the point scale following the procedure described in the previous sections. The Weibull distribution is fitted by means of the probability weighted moments approach (Greenwood et al., 1979), following Zorzetto et al. (2016).

While the size of the estimation window over which Weibull parameters are estimated (not to be confused with the blocks over which maxima are determined, which typically remain yearly in applications) can in general be varied, we limit here our analysis to yearly estimates. We note that in the case of very dry climates (i.e., low number of events/year) this choice may not be optimal, and longer windows could improve parameter estimation. On the other hand, using estimation windows that are longer than necessary is not advantageous as it reduces the variability of extremes associated with interannual variabilities (and, possibly, with systematic long-term changes). We suggest that such metastatistical source of variability in the ordinary events plays an important role in the emergence of fat-tailed extreme values (Zorzetto et al., 2016). This is in general justified as the rainfall process is the result of a mixture of different mechanisms that appear every year with different frequencies and thus determine a variation in shape and scale parameters of the parent distribution of ordinary rainfall values.

2.5. Satellite Rainfall Data

The Tropical Rainfall Measurement Mission (TRMM) Multisatellite Precipitation Analysis (TMPA) 3b42 data set provides a 19-years long, quasi-global coverage of tropical and subtropical regions (Latitudes between −50°S and +50°N), with remarkable spatial (0.25° × 0.25°) and temporal (3-hourly) resolution. The TMPA 3b42 version 7, research-quality, data set provided by NASA and used in this study can be accessed at

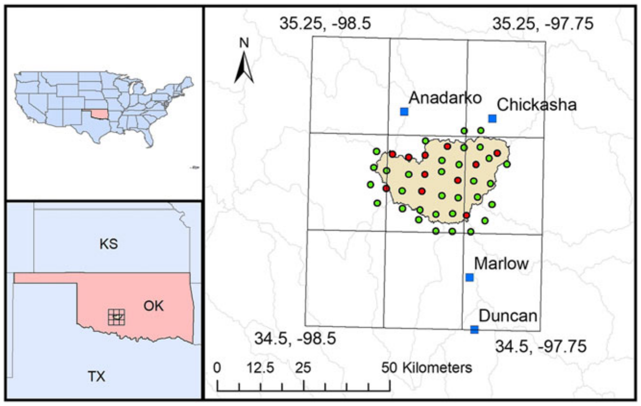

Figure 2. Schematic map of the Tropical Rainfall Measuring Mission Multisatellite Precipitation Analysis (TMPA) pixels and of the rain gauge network used in this study. The rain gauges in the Micronet Network are represented by circles (red filled circles indicate stations with a complete 1998–2015 record, and green circles for rain gauges with shorter time series), while blue squares represent the locations of the 4 Global Historical and Climatology Network stations with longer records. The black grid represents the boundaries of the the TMPA pixels used in the analysis. The coordinates of the corners of the TMPA domain are also reported.

https://mirador.gsfc.nasa.gov/. TMPA estimates are obtained by merging information from a set of different sensors (primarily passive microwave and infrared) characterized by differing accuracy and resolution, with the purpose of improving the overall quality and coverage of the final (level 3) product. As a final step, ground-based gridded precipitation data from the Global Precipitation Climatology Project (GPCP) are used to correct TMPA precipitation estimates to preserve ground-estimated monthly means (see Huffman et al., 2007, for details). For the purpose of this study, we extracted a lattice of 3×3 TMPA pixels centered at the point with coordinates 34.785N, −98.125E (see Figure 2) to match the ground-based data used for testing and validation of the methods. TMPA 3b42 gridded rain rate fields are available every 3 hr. Here we regard these values as average quantities over the observation interval. After correcting for the local time zone (since data are reported at a nominal observation time), we compute daily totals based on the 3-hourly rainfall rates. The complete TMPA record in the interval 1998–2015 was used in the analysis, after testing that for each QPE time series the yearly fraction of missing data was less than 10%. Missing data values were set to 0.

2.6. Ground-Based Observations

To test estimates of point-value extremes from TMPA data, we take advantage of a dense rain gauge network (ARS Micronet), located in the Little Washita River watershed, Oklahoma (Elliott et al., 1993). The network consists of 42 tipping bucket rain gauges, 23 of which fall within one single pixel of the TMPA 3b42 gridded product (see Figure 2). This particular network was selected to test our methodology because of (i) the remarkable spatial density of the stations and (ii) the extensive characterization of TMPA performance available for this particular location (e.g., Hossain & Huffman, 2008; Villarini & Krajewski, 2007). We identify and use for our analysis a subset of the rain gauges in the network that fall within a single TMPA pixel and for which a continuous 19-year record exists (1998–2016), providing a perfect temporal overlap with the TMPA data set. The daily data from the Oklahoma Micronet were obtained from http://ars.mesonet.org/ and were preprocessed by removing data that the were marked as affected by certain or highly probable instrumental error (Elliott et al., 1993).

For testing downscaling results with ground observations, we use the Micronet time series for which an almost complete record exists in the interval 1998–2015, so as to match exactly the temporal range of TMPA QPEs. Of the 23 Micronet stations over the pixel centered in 34.785N, −98.125E, only seven have a continuous record in this range of years (with a maximum number of missing values/year less than 42). We use this subset of the stations to fit the distribution of daily rainfall accumulations at a point and to compare it with the corresponding TMPA pixel-average and downscaled distributions. For testing the TMPA-downscaled spatial correlation function, all stations in the Micronet network are used.

Due to the limited length of the TMPA data set used in this study, it is desirable to use an independent, and longer, set of observations in close proximity to the Micronet, to be able to empirically evaluate quantiles with relatively large return periods. For this reason, we selected four stations from the National Oceanic and

Table 1
Summary of the GHCND Stations Used to Validate Downscaled High-Return Period Rainfall Values Obtained From TMPA Data

Station	GHCND station ID	Latitude	Longitude	Elevation	Time span
Anadarko	USC00340224	35.0667	−98.25	354.8	1893–2016
Chickasha	USC00341747	35.05	−97.95	332.5	1901–1965
Chickasha	USC00341750	35.05	−97.91667	331.9	1954–2016
Duncan	USC00342660	34.5011	−97.9591	343.2	1936–2016
Marlow	USC00345581	34.6368	−97.9786	393.8	1900–2016

Note. GHCND = Global Historical and Climatology Network Daily; TMPA = Tropical Rainfall Measuring Mission Multisatellite Precipitation Analysis.

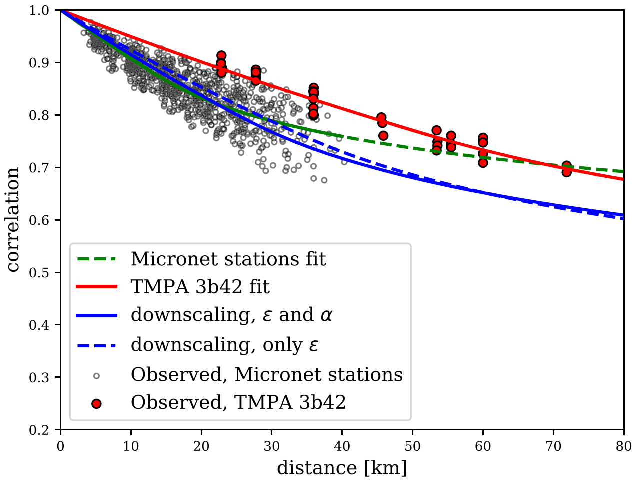

Figure 3. Comparison of rainfall correlation function in space as computed from the rain gauges in the Micronet network (open circles) and TMPA gridded precipitation (red circles). Fit of the exponential kernel model is shown by the green dashed line and red line for rain gauges and TMPA correlations, respectively. Result of the downscaling scheme is also indicated (blue line). The result obtained by only downscaling the scale parameter while is also reported for comparison (blue dashed line). TMPA = Tropical Rainfall Measuring Mission Multisatellite Precipitation Analysis.

Atmospheric Administration (NOAA) Global Historical and Climatology Network Daily (GHCND) data set (see Table 1). For each station, only years with less than 10% of missing years were included in the analysis. The stations were selected on the basis of (i) the length of the record (set to be at least 50 years) and (ii) their proximity to the Micronet stations. As shown in the following, the precipitation field is still highly correlated at distances larger than the maximum distance between these stations, suggesting that observations from the GHCND gauges and the Micronet stations can be regarded as samples of the same rainfall process.

3. Results

3.1. Correlation Structure and Downscaling of Daily Rainfall Distribution

We start by comparing the spatial correlation function computed from the 9 TMPA time series corresponding to the pixels covering the study area, the downscaled point correlation function obtained by the minimization of equation (16), and the correlation independently estimated using the Micronet rain gauges at the ground (Figure 2). The analysis of interstation correlation for the Micronet network reveals that this site is characterized by a slowly decaying correlation (Figure 3). The values of the parameters defining the correlation model indicate a decay slower than predicted by a simple exponential (the transition to power-law behavior occurs at about $\epsilon = 14$ km, see Table 2), suggesting caution in using the common exponential correlation functions arising from spatial Poisson models (Cox & Isham, 1988; Del Jesus et al., 2015). The rainfall fields obtained from the TMPA 3b42 data set exhibit greater spatial correlation than those from the point process, as expected. To test how well the correlation structure of the continuous rainfall field can be reconstructed based on TMPA data alone, we minimize the SSE and determine the parameters (ϵ and α) describing the point to point correlation. Figure 3 shows that the proposed downscaling procedure yields correlation values which are consistent with the point correlation values estimated from the Micronet network observations (see Table 2 for the specific parameter values). For distances larger than 40 km (extrapolating beyond the range of distances available for fitting the spatial correlation function), the downscaled correlation model appears to decay faster than the one obtained from fitting the point observations.

This evidence confirms the importance of correctly accounting for the area-averaged nature of remotely sensed information when comparing correlation functions from satellite and ground-based precipitation observations. The downscaling exercise was also repeated by keeping the exponent α constant across scales, and by solving the optimization of equation (16) only to determine the value of ϵ, the scale parameter of the correlation function at a point. This yielded a similar result to the one obtained by minimizing both parameters (Figure 3). Application of equation (3) using the TMPA-downscaled spatial correlation function yielded a value of the variance reduction function $\gamma_0(L) = 0.89$ between the pixel and the point scale.

Next, we compare the values of the intermittency ratio β_0 obtained by applying Taylor's hypothesis as described in section 2.3 with ground and satellite observations averaged at different scales. The procedure

Table 2
Parameters ϵ (Scale) and α (Shape) of the Exponential Kernel Model Describing the Spatial Correlation Structure of Daily Rainfall

Data set	ϵ (km)	α
Micronet stations network	13.75	0.13
TMPA 3b42 pixels	53.14	0.28
Downscaling from TMPA, α and ϵ	26.50	0.23
Downscaling from TMPA, only ϵ	34.79	0.28

Note. TMPA = Tropical Rainfall Measuring Mission Multisatellite Precipitation Analysis.

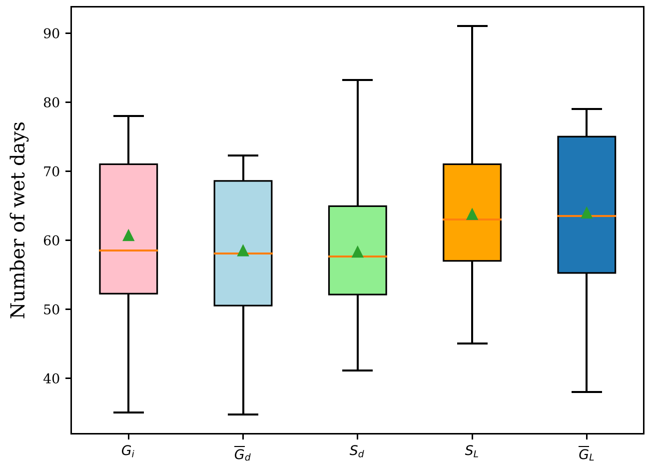

Figure 4. The results of downscaling for the wet fraction p_r. The distribution of the yearly number of wet days observed for the Micronet stations (pink, G_i), for their pixel average (blue, $\bar{G}_L$), and for the TMPA time series at the same location (orange, S_L). The downscaled values at a point obtained from the gauge average $\bar{G}_d$ and from the TMPA data S_d are included in cyan and green, respectively. The boxplots report the mean (green triangles) and median (orange line) of each distribution. The bars extend from the lower to the upper distributional quartiles, and the whiskers represent the range of each sample. TMPA = Tropical Rainfall Measuring Mission Multisatellite Precipitation Analysis.

based on the Taylor hypothesis yields a value of $\beta_0(L) = 1.09$, slightly larger than the value obtained by averaging the intermittency ratio from Micronet time series measured at the ground ($N_L/N_0 = 1.05$). Figure 4 shows a comparison of the yearly number of wet days distribution observed at the ground (Micronet stations) with the corresponding values at the pixel scale. The distribution of N_L obtained from TMPA QPEs (S_L) and by averaging rain gauges at the ground ($\overline{G_L}$) both exhibit a larger mode when compared to the point values observed at single rain gauges (G_i). We then apply the Taylor hypothesis to also obtain estimates of the number of wet days N_0 at a point in space. The distributions of N_0, obtained respectively from downscaling gauge average ($\overline{G_d}$) and TMPA QPEs (S_d), exhibit lower mean and median than the original distributions of N_L, yielding results consistent with the distribution of values observed by rain gauges at the ground.

We next illustrate the application of the downscaling approach to the transformation of the pdf of rainfall values averaged/observed at a coarse scale to the pdf of rainfall values at a finer spatial scale. Before applying the method to infer extreme value statistics at a point, we first test how well the method reproduces the distribution of ordinary rainfall values at different spatial scales. To do so, we apply the downscaling method to Weibull parameters obtained fitting the entire available satellite and rain gauge time series. To downscale these probability distributions of ordinary events, we proceed as follows. At the coarse scale, the Weibull parameters are estimated by means of the probability weighted moments technique (Greenwood et al., 1979). We then estimate the values of the parameters at the point scale by use of the downscaling relations, equations (10) and (11), using the values of β_0 and γ_0 obtained from TMPA time series.

We first select the Micronet stations within the pixel centered in 34.875N, −98.125E (central pixel in Figure 2) with at least 18 years of data, in order to obtain a perfect overlapping with the time interval of the TMPA data set and compute their average time series. The downscaling procedure is then applied to this "exact" areal average rainfall to test whether the approach can recover the distribution of daily rainfall accumulations at a

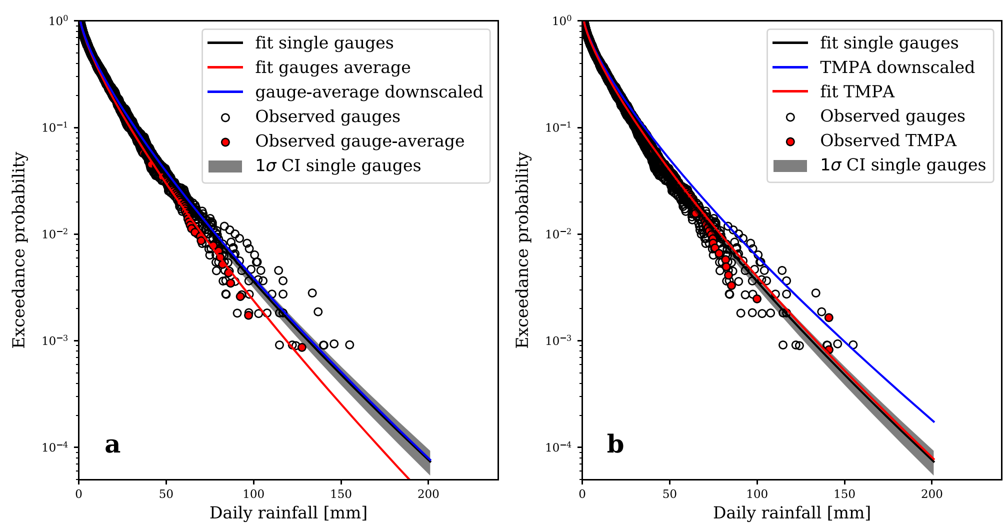

Figure 5. (a) Exceedance probability distributions observed for single Micronet stations with at least 19 years of data (open circles) and from their pixel average (red circles). The Weibull fits are reported in red for the average, and black for the single station (mean and 1σ standard deviation confidence interval). The blue line shows the distribution obtained by downscaling from the pixel scale to a point. (b) Comparison of the same exceedance probability distribution for Micronet stations (open circles) and satellite observations (red circles), and the respective Weibull fit (red line and black area, respectively). The blue line represent the probability distribution downscaled from the satellite data set. TMPA = Tropical Rainfall Measuring Mission Multisatellite Precipitation Analysis.

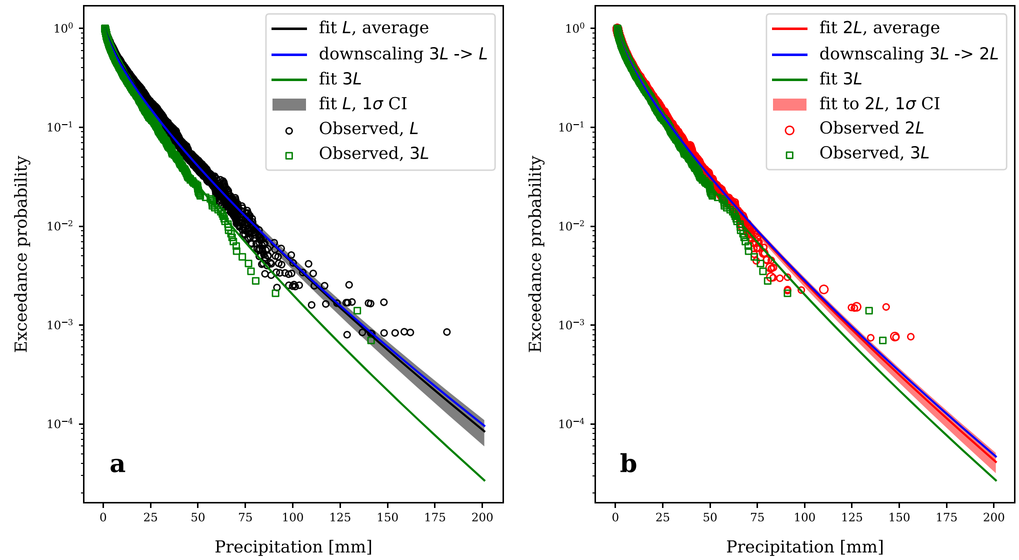

Figure 6. (a) Exceedance probability distributions observed for Tropical Rainfall Measuring Mission Multisatellite Precipitation Analysis time series aggregated spatially at different scales. (a) Results for the downscaling from scale $3L$ to scale L, and (b) downscaling from scale $3L$ to $2L$.

point. Results show that the downscaling procedure provides a good estimation of the distribution at a point (Figure 5a), which is within the range of variability of the Micronet stations at the ground. Comparison with the TMPA daily time series over the same pixel shows that its distribution closely resemble the one obtained from data observed at a point (Figure 5b). In both cases, the magnitude of the scale correction directly depends on the decay of the correlation function, which exhibits a long tail.

Given the large spatial extent of the correlation over the study area, and in order to more stringently test the downscaling approach formulated here, we consider progressively coarser data obtained by averaging over 2×2 pixels (linear characteristic scale $2L$) and over 3×3 pixels (scale $3L$) centered in −98.125E, 34.785N (see lattice in Figure 2). Again, in order to test the downscaling method using homogeneous observations at different scales, we focus our attention on satellite estimates only, performing the downscaling from scale $3L$ to scale L (a single pixel) and from $3L$ to $2L$. This application of the downscaling method confirms that the methodology, even when applied to the coarse observations at the $3L$ scale, is able to correctly reproduce the exceedance probability distribution at smaller spatial scales (downscaling from scale $3L$ to scales L and $2L$ are featured in Figures 6a and 6b respectively). The shape of the exceedance probability distribution changes more markedly in this case, as large values become significantly less likely at coarser aggregation scales (see green and red lines in Figure 6). Overall, we find a better performance when the method is applied and tested using homogeneous data (using either TMPA QPEs or gauges averaged at different spatial scales), while some discrepancy exists when gauge and satellite data are compared, as in Figure 5b. These findings suggest that such added differences can be attributed to observational limitations affecting remote sensing QPE values.

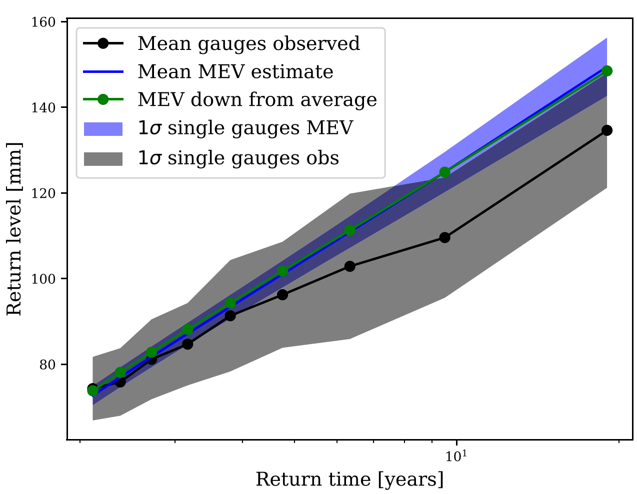

Figure 7. Extreme values observed and estimated for the Micronet stations within the TMPA pixel centered in 34.785N, −98.125E. Observed annual maxima from the Micronet stations with 19 years of data (black, mean and 1σ confidence interval), quantiles estimated from MEVD fitted directly to time series at a point (blue, mean and 1σ confidence intervals), and from downscaling Weibull parameter values from the pixel-average time series (green circles). MEVD = Metastatistical Extreme Value distribution.

3.2. Extreme Value Analysis

After testing how the distributions of ordinary values can be reconstructed at a small spatial scale given knowledge of the distribution at the TMPA pixel scale, we now turn to the inference of the extreme value distribution at the point scale. We first apply MEVD to the stations of the Little Washita Micronet, despite the short record length available. In this case, the empirical quantiles observed at the ground appear to be somewhat

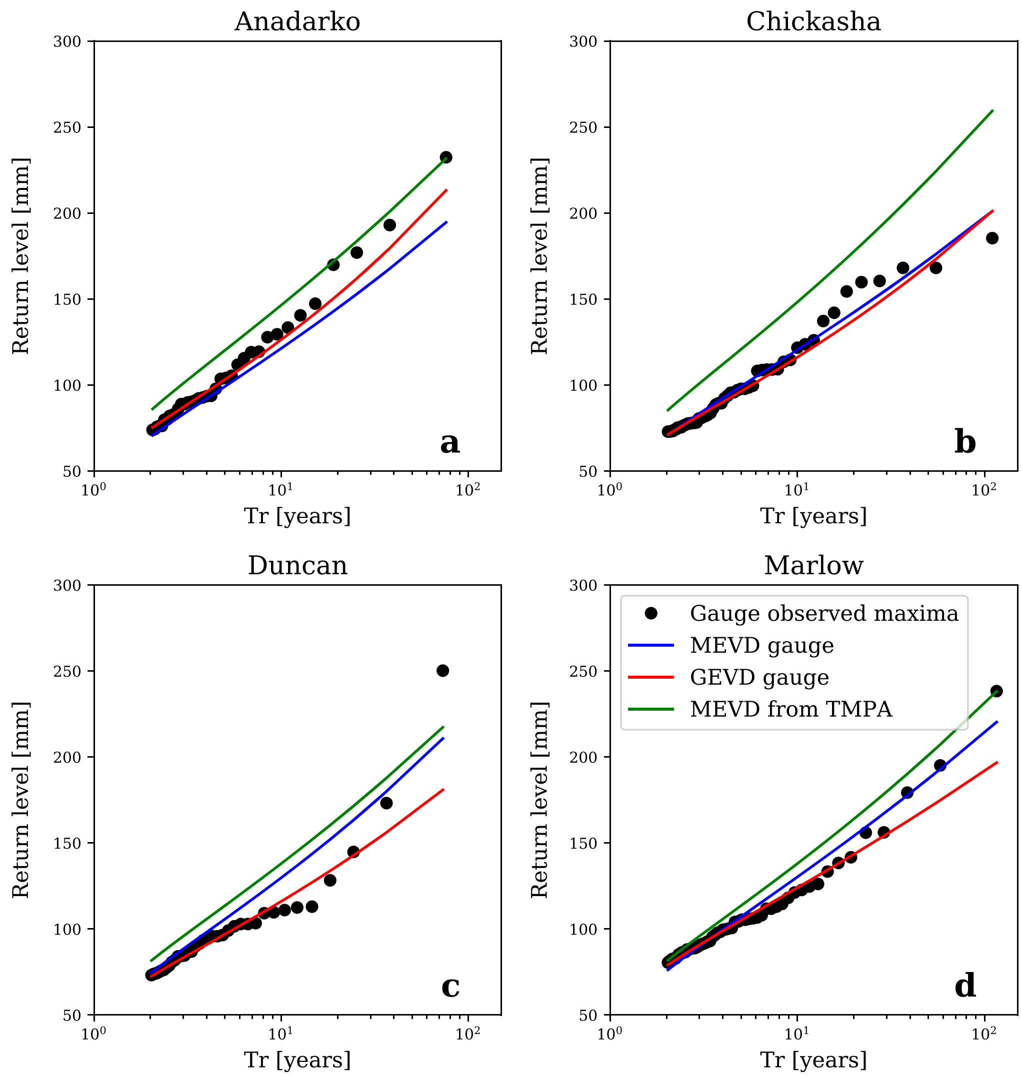

Figure 8. Extreme quantiles observed for the four GHCN stations in the vicinity of the Micronet network (black markers). The corresponding estimated quantiles have been obtained from directly fitting the extreme value models GEVD (red lines) and MEVD (blue lines) to the entire observed time series. Green lines show the corresponding MEVD quantiles obtained by fitting the Weibull distribution to corresponding TMPA pixel time series and by downscaling the yearly Weibull parameters in the MEVD expression to the point scale. MEVD = Metastatistical Extreme Value distribution; GEVD = Generalized Extreme Value distribution; TMPA = Tropical Rainfall Measuring Mission Multisatellite Precipitation Analysis; GHCN = Global Historical and Climatology Network.

overestimated (Figure 7), similarly to what happens when downscaling the Weibull parameters from the pixel-average time series. We explain this behaviour by recalling that the MEVD yields an optimal performance when the return time for which a quantile is estimated is greater than the sample size used for the estimation (e.g., see Zorzetto et al., 2016). In the present case the same sample is used for both calibration and validation, and the relatively short sample limits the range of return times that can be explored in the comparison with ground observations.

Hence, to more accurately investigate the performance of the proposed model over a wider range of return times, we compare MEVD downscaling results with those obtained from rain gauge stations from the GHCND network, with record lengths ranging from 72 to 115 years (Table 1). For each station, the corresponding TMPA pixel time series was used to fit the Weibull distribution and estimate the values of parameters C_L and w_L, which were subsequently downscaled to the point scale (C_0 and w_0). Downscaled parameter values were used to construct the MEVD according to equation (18) and estimate quantiles for a set of return times up to the length of the available time series. Comparisons are then performed with the empirical quantiles, that is,

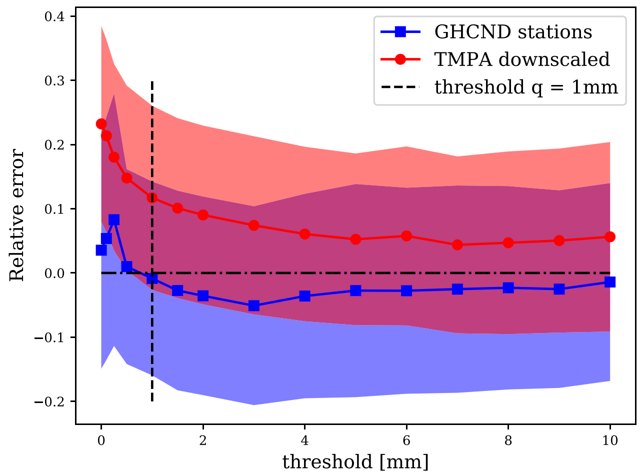

Figure 9. Effect of the detection threshold used to define ordinary rainfall values on extreme value estimates for a return times of Tr = 15 years. The relative error is reported for TMPA-downscaled estimates (red) and GHCND stations (blue). Solid lines and shaded areas refer to average and 1σ intervals over the four stations. GHCND = Global Historical and Climatology Network Daily; TMPA = Tropical Rainfall Measuring Mission Multisatellite Precipitation Analysis.

the actual AM observed. Results are also comparatively evaluated with estimates obtained by directly fitting GEVD and MEVD to rain gauge-measured time series (Figure 8). High quantile estimates obtained fitting GEVD and MEVD (to time series of AM and ordinary rainfall events, respectively) both exhibit a good match with the empirical quantiles extracted from the same time series. While some overestimation of extreme quantiles is still seen for one of the stations for estimates downscaled from TMPA QPEs, the comparison with longer observational time series shows a good match with empirical quantiles.

The effect of the specific detection threshold used to detect ordinary rainfall events is also evaluated (Figure 9). For small values of the threshold ($q <$ 1 mm), the estimated quantiles seem to depend on the particular value of the threshold used in the analysis. In particular, this variation is more significant for the TMPA data when compared to the GHCND estimated quantiles. This difference is explained by considering that rainfall values are only recorded at finite intervals by the tipping bucket rain gauges, while discretization effects are negligible for TMPA QPEs. Significantly, variations in QPE-based quantile estimates are modest when one considers values of the threshold of 1 mm or larger. For this reason we have limited our analysis to the value q = 1 mm, within the range of values in which results are weakly dependent on the specific threshold value adopted and justified by a largely used definition of "wet day."

The considerable length of the GHCND records allows us to further quantify model performance using independent samples for calibration and testing. For each station, observations are resampled with resubstitution to generate realizations that preserve the set of parameters (N, C, w) from the original time series. Subsequently, the synthetic time series thus obtained are divided into two independent subsamples, of which one is used for calibration and one for testing. The test was performed by extracting from test samples the AM and by estimating the corresponding return times by means of the Weibull plotting position formula (e.g., see Zorzetto et al., 2016). This procedure was repeated for a number of times n_g = 100. For each such bootstrap realization, observed (h^{obs}) and estimated quantiles for a given return time ($\hat{h}(Tr)$) were used to compute a

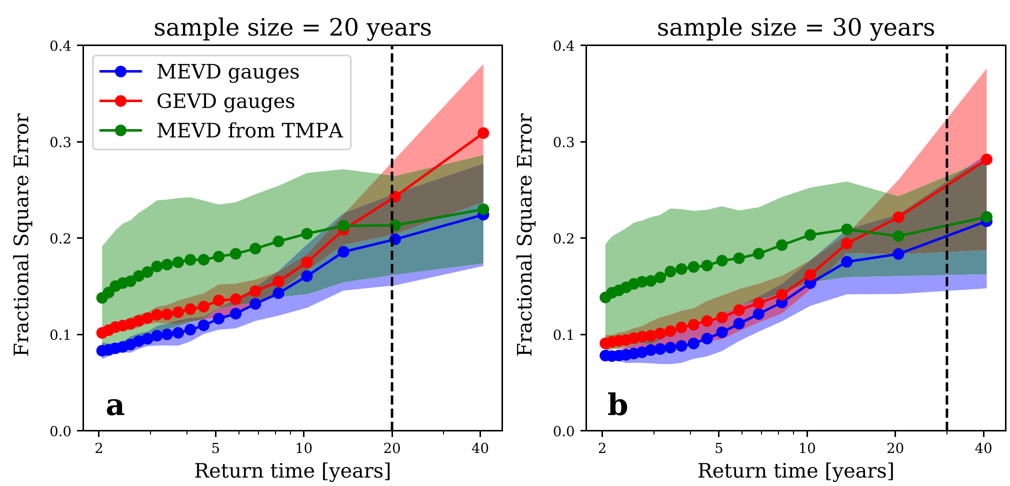

Figure 10. Fractional square error obtained from the cross-validation test using samples of 20 years (a) and 30 years (b) in fitting MEVD (blue) and GEVD (red) to rain gauge GHCND data. The results from the application of the MEVD distribution calibrated from TMPA observations and downscaled at a point is reported in green for both panels. Lines and shaded areas depict averages and standard deviations respectively, computed by repeating the procedure for the set of GHCND stations. Vertical dashed lines indicate the value of the return time corresponding to the sample size used for calibration of MEVD and GEVD with rain gauge data. MEVD = Metastatistical Extreme Value distribution; GEVD = Generalized Extreme Value distribution; TMPA = Tropical Rainfall Measuring Mission Multisatellite Precipitation Analysis.

fractional square error (FSE), defined as

$$FSE(s, Tr) = \left(\frac{1}{n_g} \sum_{i=1}^{n_g} \left[\frac{\hat{h}_i(Tr) - h_i^{obs}(s_s, T_r)}{h_i^{obs}(T_r)} \right]^2 \right)^{1/2} \quad (19)$$

where s is the calibration sample size and Tr is the return time. This procedure was here applied to rain-gauge calibration samples with length 20 and 30 years, respectively, representative of the typical satellite record length, and for values of Tr up to 40 years (limited by the available test sample sizes).

The entire bootstrap procedure was then repeated using the downscaled parameters obtained from the TMPA record, and again using a set of $n_g = 100$ synthetic samples of 40 years, randomly extracted from the relevant GHCND station for testing. In this case only the validation sample (randomly extracted from a GHCND station at the ground) varied, while the calibration sample was kept constant (corresponding to the entire TMPA time series available).

The results of this analysis (Figure 10) show that the performance of MEVD and GEVD calibrated using rain gauge data are comparable for small values of the return time (up to about $Tr = 15$ years for the sample size of $s = 20$ years, and to about $Tr = 20$ years in the case of $s = 30$ years). In essence, the advantage in using the MEVD over the GEVD distribution becomes evident for values of Tr greater than the length of the sample used for calibration, as found in previous work (Zorzetto et al., 2016). The extreme values estimates obtained by downscaling TMPA statistics to the point scale (green line in Figure 10) yield values of the FSE which are consistently higher when compared to ground observations, as one would expect. However, as the return time increases, the error increases at a rate that is lower than that characterizing ground-based estimates, and results are comparable for return times of 20 years and larger. In this range of return times, estimation uncertainty is particularly large for the GEVD model, as observed when calibration and validation are performed using independent data sets. We note that this result was obtained without applying any bias correction to the TMPA-derived distribution of rainfall accumulations. Overall, these results support the robustness of the method proposed, when applied to relatively short time-series record, as is the case for the TMPA data set, and when relatively high quantiles need to be estimated.

4. Discussion and Conclusions

We developed and tested a new downscaling approach to infer point rainfall extreme value distributions from satellite observations. The approach, outlined in sections 2.1–2.5, introduces a stochastic framework that provides estimates of "ordinary" and extreme value probability distributions at the point scale. The procedure is parsimonious and its application only requires (1) the specification and fitting of the probability distribution of "ordinary" values observed at the coarse aggregation scale; (2) knowledge of the correlation structure of the rainfall field as observed from remote sensing at the coarse scale; and (3) knowledge of the intermittency structure of rainfall events as quantified by β_0, ratio of the wet fractions at the pixel and point scales, which can also be estimated from satellite observations using the Taylor hypothesis. A summary of the steps necessary for the application of the method is provided in Appendix A.

The use of the dense Little Washita Micronet rain gauge network allowed some detailed testing of the proposed approach. In particular, we performed downscaling tests from/to the following spatial scales: 75 km (3×3 TMPA pixels), 25 km (1 TMPA pixel), and the point scale (rain gauges). The ordinary and extreme value distributions downscaled from coarser scale observations exhibit a good agreement with those obtained from observations at target (smaller) scales when homogeneous observations (either rain gauges or TMPA QPE fields) averaged at different spatial scales are used. When the method is applied to TMPA QPEs and validated using independent ground observations, we observe some discrepancy in the downscaled probability distributions of daily rainfall. Comparison between these results (obtained by comparing downscaled TMPA statistics and rain gauges at the ground) with those obtained using homogeneous observations suggests that this behavior is primarily due to the performance of TMPA QPEs over this particular location. This result is appealing as extensive application of the method can lead to the evaluation of multisensor-derived precipitation fields over regional to global scales.

For the study location, the application of the MEVD-downscaled method to TMPA data led to errors in quantile estimates that are comparable to those obtained by application of MEVD or GEVD distribution directly to the gauge data for the largest values of return time explored here. This result is quite encouraging in terms of (1) testing remote sensing rainfall observations (and TMPA data in particular) against point observations at the ground at the global scale and (2) evaluating with reasonable and quantifiable accuracy point extremes at the global scale using TMPA (and possibly other rainfall remote sensing) observations.

While this work builds a new framework for estimating rainfall extremes from satellite data, a significant result with many hydrological applications, a number of hypotheses are made. First, the assumption of isotropic correlation structure, while commonly used, could limit the application of the method, for example, in the presence of orographic forcing. However, the covariance expression, equation (12), can in principle be adapted to different and nonisotropic forms, if additional information on the spatial correlation structure is available. This is particularly important in applications over complex terrain. The Taylor hypothesis used here has also been derived for an homogeneous fields advected by a mean velocity field, and its application should be carefully evaluated over heterogenous terrains, and in location characterized by intense localized events where the average advection velocity is very low, as can be the case in mountainous areas. However, we note that the methods presented here can be directly applied to higher-resolution satellite products, and in particular to the IMERG data set, as longer time series become progressively available. The application to data sets with higher spatial resolution is likely to reduce the effects of the assumptions made here for the covariance of the rainfall process and the wet fraction (Taylor hypothesis). Where rain gauges at the ground are available, their information could also be incorporated in the downscaling procedure and used to improve the estimation of β_0 and the correlation function at a point. This information could be used even when a few stations are available at the location of interest, which would not be enough to compute pixel-average properties for direct comparison with TMPA QPEs.

The downscaling method proposed assumes that the form of the probability distribution of rainfall values (Weibull in this case) is preserved across different spatial scales. While it is known that this is not rigorously the case, our results suggest that this assumption approximately holds in the range of scales explored here (linear scales ranging from 0.1 m up to about 75 km).

We tested our approach in a region which is characterized by a relatively simple orography, where a dense network of ground observations is available for independent testing and where TMPA uncertainty is relatively well characterized in the absence of additional confounding factors (e.g., large variability in surface emissivity and high relief). It will be important to further test the proposed method, which is general in nature and can potentially be applied to any multisensor satellite QPE product, by exploring a wider set of locations with different rainfall regimes. In particular, applications to coastal areas, tropical climates and locations with high relief will be particularly challenging, for the coexistence of different precipitation mechanisms and severe storms likely to affect the shape of the daily rainfall pdf as well as the performance of TRMM sensors (Li et al., 2018; Rossow et al., 2013).

In applying the proposed approach at larger scales, we note that, because the downscaling procedure connects satellite- and point-scale probability distributions, it can also be used to correct the satellite-inferred ordinary distribution and MEVD in data-scarce regions where only sparse rain gauges are available. Even in the presence of a single rain gauge in a given location, it would be possible to compare satellite-derived point rainfall statistics (β_0, γ_0, and Weibull parameters) with the corresponding values observed at a point. The approach can thus potentially lead to a self-contained procedure, yielding internal bias correction as well as high quantile rainfall estimates.

The scale-wise dependence of the distribution of daily rainfall was here combined with the MEVD framework to infer extreme value properties of the rainfall field at a point in space. The downscaling approach presented here can improve extreme rainfall estimation in data-scarce regions, where information from satellite QPEs can now be employed at subpixel scales. The link proposed here between key statistical properties of the rainfall process at different spatial scales has broad implications for hydrological and ecological watershed studies, with the broader goal of better understanding the global distribution of hydrologic extremes over a wide range of scales.

Appendix A: Variance of the Compound Process

The compound rainfall process (wet and dry periods) is characterized by a pdf $f_c(h)$ that has a finite atom of probability in $h = 0$, such that $f_c(h) = (1 - p_r)\delta(h) + p_r f_r(h)$, where $f_r(h)$ is the pdf of wet events only, $\delta(h)$ is the Dirac delta function centered in 0, and p_r is the probability of a day being wet. Therefore, the mean of the compound process is $\mu_c = \mu_r p_r$ as there is no contribution from the atom of probability in zero. The variance is

$$\sigma_c^2 = E\left[\left(h - \mu_c\right)^2\right] = E\left[h^2\right]_c - E\left[h\right]_c^2 \tag{A1}$$

where $E[\cdot]$ is the expected value operator. Therefore,

$$\sigma_c^2 = (1 - p_r)\int_0^{\nu} h^2 \delta(h - 0)dh + p_r \int_{\nu}^{+\infty} h^2 f_r(h)dh - E\left[h\right]_c^2 \tag{A2}$$

in the limit $\nu \rightarrow 0$. Since the value of the first integral in equation (A2) is zero, one obtains

$$\sigma_c^2 = p_r E\left[h^2\right]_r - p_r^2 \mu_r^2 \tag{A3}$$

from which, summing and subtracting $p_r \mu_r^2$

$$\sigma_c^2 = p_r E\left(\left[h^2\right]_r - \mu_r^2\right) + p_r \mu_r^2 - p_r^2 \mu_r^2 \tag{A4}$$

thus proving equation (5)

$$\sigma_c^2 = \sigma_r^2 p_r + \mu_r^2\left(1 - p_r\right)p_r \tag{A5}$$

Appendix B: Summary Description of the Downscaling Methodology

1. Extraction of the local lattice of TMPA 3b42 pixels QPEs time series at the 3-hourly time scale, centered over the location of interest.
2. Aggregation of TMPA data at the daily scale, construction of the time series of exceedances over the detection threshold, evaluation of the cross correlation between the TMPA QPEs time series, and minimization of equation (16) in order to estimate the parameters α and ϵ defining the point correlation function.
3. Application of the procedure detailed in section 2.3 to estimate the quantity β_0 using Taylor's frozen turbulence hypothesis.
4. Evaluation of the the variance reduction function equation (3) by integrating the correlation function $\rho(d; \alpha, \epsilon)$ at a point.
5. Estimation of the yearly parameters C_L and w_L by fitting the Weibull distribution to the TMPA QPE time series over the location of interest.
6. Downscaling of the yearly parameters of the Weibull distribution at a point (C_0 and w_0) using equations (10) and (11).
7. Numerical inversion of the MEVD nonexceedance probability expression equation (18) to compute extreme value quantiles $\hat{h}(Tr)$ for the desired return time.

Notation

$\boldsymbol{i}$	instantaneous rainfall rate at a point (mm/hr)
$\boldsymbol{L_x}, \boldsymbol{L_y}$	effective linear dimensions of a TMPA pixel (km)
$\boldsymbol{L}$	characteristic linear dimension of a TMPA pixel (km)
$\boldsymbol{T}$	generic time integration interval (hr)
$\boldsymbol{X}$	generic linear characteristic averaging scale (km)
$\boldsymbol{U}$	advection speed (km/hr)
$\boldsymbol{T_d}$	(=24 hr) daily time integration interval
$\boldsymbol{h}$	daily rainfall accumulation at a point (mm)
$\boldsymbol{h_L}$	daily rainfall accumulation at the pixel scale (mm)
$\boldsymbol{p_r}$	yearly fraction of rainy days
$\boldsymbol{\mu_r^2}$	mean of wet process (mm)
$\boldsymbol{\sigma_r^2}$	variance of wet process (mm^2)
$\boldsymbol{\gamma_0(L)}$	variance function
$\boldsymbol{\beta_0(L)}$	intermittency function
$\boldsymbol{\beta(L_1, L_2)}$	intermittency function between two generic scales

$\gamma(L_1, L_2)$	variance function between two generic scales
$\rho(x,y)$	autocorrelation function at a point
d	distance between two points in space (km)
$\rho_{h_L,h'_L}(d)$	correlation of local averages
ρ_j	Pearson correlation between two TMPA time series at distance d_j.
Δ	Integral variance function
$F(h)$	cumulative distribution function of ordinary rainfall
$\zeta(h)$	cumulative distribution function of extreme rainfall
w	Weibull shape parameter
C	Weibull scale parameter (mm)
$\vec{\theta}$	Generic set of parameters of the MEV distribution
N	yearly number of rainy days (days)
ϵ	autocorrelation function scale parameter (km)
α	autocorrelation function shape parameter
s	sample size (years)
T_r	return time (years)
FSE	fractional square error
SSE	sum of square errors
q	rainfall detection threshold (mm)
y	excesses over threshold (mm)
n_g	number of resamplings for bootstrapping

Acknowledgments
The authors acknowledge support from the National Aeronautics and Space Administration NESSF 17-EARTH17F-0270 and from the National Science Foundation grant NSF-EAR-13-44703 "The Direct and Indirect Effects of Plantation Forestry Expansion on Usable Water in the Southeastern US." The data sets used in this study are available online at https://mirador.gsfc.nasa.gov/ (TMPA data), https://www.ncdc.noaa.gov/ (GHCND station data), and http://ars.mesonet.org/ (Micronet station data).

References

Bell, T. L. (1987). A space-time stochastic model of rainfall for satellite remote-sensing studies. *Journal of Geophysical Research*, *92*(D8), 9631–9643.

Byrd, R. H., Lu, P., Nocedal, J., & Zhu, C. (1995). A limited memory algorithm for bound constrained optimization. *SIAM Journal on Scientific Computing*, *16*(5), 1190–1208.

Camuffo, D., Bertolin, C., Diodato, N., Cocheo, C., Barriendos, M., Dominguez-Castro, F., et al. (2013). Western mediterranean precipitation over the last 300 years from instrumental observations. *Climatic change*, *117*(1-2), 85–101.

Coles, S., Bawa, J., Trenner, L., & Dorazio, P. (2001). *An introduction to statistical modeling of extreme values*. London: Springer.

Cowpertwait, P., Kilsby, C., & O'Connell, P. (2002). A space-time Neyman-Scott model of rainfall: Empirical analysis of extremes. *Water Resources Research*, *38*(8), 1131. https://doi.org/10.1029/2001WR000709

Cox, D., & Isham, V. (1988). A simple spatial-temporal model of rainfall. *Proceedings of the Royal Society of London A: Mathematical, Physical and Engineering Sciences*, *415*, 317–328.

Deidda, R. (2000). Rainfall downscaling in a space-time multifractal framework. *Water Resources Research*, *36*(7), 1779–1794.

Del Jesus, M., Rinaldo, A., & Rodríguez-Iturbe, I. (2015). Point rainfall statistics for ecohydrological analyses derived from satellite integrated rainfall measurements. *Water Resources Research*, *51*, 2974–2985. https://doi.org/10.1002/2015WR016935

Eggert, B., Berg, P., Haerter, J., Jacob, D., & Moseley, C. (2015). Temporal and spatial scaling impacts on extreme precipitation. *Atmospheric Chemistry and Physics*, *15*(10), 5957–5971.

Elliott, R., Schiebe, F., Crawford, K., Peter, K., & Puckett, W. (1993). A unique data capability for natural resources studies. In *International Winter Meeting of the American Society of Agricultural Engineers* (pp. 14–17). Chicago, IL.

Frisch, U., & Sornette, D. (1997). Extreme deviations and applications. *Journal de Physique I*, *7*(9), 1155–1171.

Gebremichael, M., & Krajewski, W. F. (2004). Assessment of the statistical characterization of small-scale rainfall variability from radar: Analysis of trmm ground validation datasets. *Journal of Applied Meteorology*, *43*(8), 1180–1199.

Gnedenko, B., & Kolmogorov, A. (1954). *Independent random variables Cambridge*. Massachusetts: Addison-Wesley.

Greenwood, J. A., Landwehr, J. M., Matalas, N. C., & Wallis, J. R. (1979). Probability weighted moments: Definition and relation to parameters of several distributions expressable in inverse form. *Water Resources Research*, *15*(5), 1049–1054.

Gupta, V. K., & Waymire, E. C. (1993). A statistical analysis of mesoscale rainfall as a random cascade. *Journal of Applied Meteorology*, *32*(2), 251–267.

Habib, E., Krajewski, W. F., & Ciach, G. J. (2001). Estimation of rainfall interstation correlation. *Journal of Hydrometeorology*, *2*(6), 621–629.

Haerter, J. O., Eggert, B., Moseley, C., Piani, C., & Berg, P. (2015). Statistical precipitation bias correction of gridded model data using point measurements. *Geophysical Research Letters*, *42*, 1919–1929. https://doi.org/10.1002/2015GL063188

Hossain, F., & Huffman, G. J. (2008). Investigating error metrics for satellite rainfall data at hydrologically relevant scales. *Journal of Hydrometeorology*, *9*(3), 563–575.

Huffman, G. J., Bolvin, D. T., Braithwaite, D., Hsu, K., Joyce, R., Xie, P., & Yoo, S.-H. (2014). Nasa global precipitation measurement (GPM) integrated multi-satellite retrievals for GPM (IMERG). Algorithm Theoretical Basis Document (ATBD), NASA/GSFC. Greenbelt, MD, USA.

Huffman, G. J., Bolvin, D. T., Nelkin, E. J., Wolff, D. B., Adler, R. F., Gu, G., et al. (2007). The TRMM Multisatellite Precipitation Analysis (TMPA): Quasi-global, multiyear, combined-sensor precipitation estimates at fine scales. *Journal of Hydrometeorology*, *8*(1), 38–55.

Kidd, C., Becker, A., Huffman, G. J., Muller, C. L., Joe, P., Skofronick-Jackson, G., & Kirschbaum, D. B. (2016). So, how much of the Earth's surface is covered by rain gauges? *Bulletin of the American Meteorological Society*, *98*, 69–78.

Kirstetter, P.-E., Hong, Y., Gourley, J., Chen, S., Flamig, Z., Zhang, J., et al. (2012). Toward a framework for systematic error modeling of spaceborne precipitation radar with NOAA/NSSL ground radar–based national mosaic QPE. *Journal of Hydrometeorology*, *13*(4), 1285–1300.

Klein Tank, A. M. G., Zwiers, F. W., & Zhang, X. (2009). Guidelines on analysis of extremes in a changing climate in support of informed decisions for adaptation, World Meteorological Organization.

Laherrere, J., & Sornette, D. (1998). Stretched exponential distributions in nature and economy: 'Fat tails' with characteristic scales. *The European Physical Journal B-Condensed Matter and Complex Systems*, *2*(4), 525–539.

Li, X., Wang, X., & Babovic, V. (2018). Analysis of variability and trends of precipitation extremes in Singapore during 1980–2013. *International Journal of Climatology*, *38*(1), 125–141.

Libertino, A., Sharma, A., Lakshmi, V., & Claps, P. (2016). A global assessment of the timing of extreme rainfall from TRMM and GPM for improving hydrologic design. *Environmental Research Letters*, *11*(5), 054003.

Marani, M. (2003). On the correlation structure of continuous and discrete point rainfall. *Water Resources Research*, *39*(5), 1128. https://doi.org/10.1029/2002WR001456

Marani, M. (2005). Non-power-law-scale properties of rainfall in space and time. *Water Resources Research*, *41*, W08413. https://doi.org/10.1029/2004WR003822

Marani, M., & Ignaccolo, M. (2015). A metastatistical approach to rainfall extremes. *Advances in Water Resources*, *79*, 121–126.

Marani, M., & Zanetti, S. (2015). Long-term oscillations in rainfall extremes in a 268 year daily time series. *Water Resources Research*, *51*, 639–647. https://doi.org/10.1002/2014WR015885

Marra, F., Nikolopoulos, E. I., Anagnostou, E. N., & Morin, E. (2018). Metastatistical extreme value analysis of hourly rainfall from short records: Estimation of high quantiles and impact of measurement errors. *Advances in Water Resources*, *117*, 27–39.

Menabde, M., & Sivapalan, M. (2000). Modeling of rainfall time series and extremes using bounded random cascades and levy-stable distributions. *Water Resources Research*, *36*(11), 3293–3300.

Menne, M. J., Durre, I., Vose, R. S., Gleason, B. E., & Houston, T. G. (2012). An overview of the global historical climatology network-daily database. *Journal of Atmospheric and Oceanic Technology*, *29*(7), 897–910.

Müller, M. F., & Thompson, S. E. (2013). Bias adjustment of satellite rainfall data through stochastic modeling: Methods development and application to Nepal. *Advances in Water Resources*, *60*, 121–134.

Nogueira, M., & Barros, A. (2015). Transient stochastic downscaling of quantitative precipitation estimates for hydrological applications. *Journal of Hydrology*, *529*, 1407–1421.

Ntegeka, V., & Willems, P. (2008). Trends and multidecadal oscillations in rainfall extremes, based on a more than 100-year time series of 10 min rainfall intensities at Uccle, Belgium. *Water Resources Research*, *44*, W07402. https://doi.org/10.1029/2007WR006471

Over, T. M., & Gupta, V. K. (1996). A space-time theory of mesoscale rainfall using random cascades. *Journal of Geophysical Research*, *101*(D21), 26,319–26,331.

Pan, M., Li, H., & Wood, E. (2010). Assessing the skill of satellite-based precipitation estimates in hydrologic applications. *Water Resources Research*, *46*, W09535. https://doi.org/10.1029/2009WR008290

Rossow, W. B., Mekonnen, A., Pearl, C., & Goncalves, W. (2013). Tropical precipitation extremes. *Journal of Climate*, *26*(4), 1457–1466.

Schertzer, D., & Lovejoy, S. (1987). Physical modeling and analysis of rain and clouds by anisotropic scaling multiplicative processes. *Journal of Geophysical Research*, *92*(D8), 9693–9714.

Stull, R. B. (1988). *An introduction to boundary layer meteorology, Atmospheric Sciences Library*. Dordrecht, Netherlands: Kluwer Academic Publishers.

Taylor, G. I. (1938). The spectrum of turbulence. *Proceedings of the Royal Society of London. Series A, Mathematical and Physical Sciences*, *164*, 476–490.

Vanmarcke, E. (1983). *Random fields: Analysis and synthesis* (394 pp.). Cambridge, MA: MIT Press.

Villarini, G., & Krajewski, W. F. (2007). Evaluation of the research version TMPA three-hourly 0.25× 0.25 rainfall estimates over Oklahoma. *Geophysical Research Letters*, *34*, L05402. https://doi.org/10.1029/2006GL029147

Villarini, G., Krajewski, W. F., & Smith, J. A. (2009). New paradigm for statistical validation of satellite precipitation estimates: Application to a large sample of the TMPA 0.25° 3-hourly estimates over Oklahoma. *Journal of Geophysical Research*, *114*, D12106. https://doi.org/10.1029/2008JD011475

Villarini, G., Mandapaka, P. V., Krajewski, W. F., & Moore, R. J. (2008). Rainfall and sampling uncertainties: A rain gauge perspective. *Journal of Geophysical Research*, *113*, D11102. https://doi.org/10.1029/2007JD009214

Wilson, P., & Toumi, R. (2005). A fundamental probability distribution for heavy rainfall. *Geophysical Research Letters*, *32*, L14812. https://doi.org/10.1029/2005GL022465

Zhou, Y., Lau, W. K., & Huffman, G. J. (2015). Mapping TRMM TMPA into average recurrence interval for monitoring extreme precipitation events. *Journal of Applied Meteorology and Climatology*, *54*(5), 979–995.

Zorzetto, E., Botter, G., & Marani, M. (2016). On the emergence of rainfall extremes from ordinary events. *Geophysical Research Letters*, *43*, 8076–8082. https://doi.org/10.1002/2016GL069445